A comparison of ARTEMIS observations and particle-in-cell modeling of the lunar photoelectron sheath in the terrestrial magnetotail

A. R. Poppe,[1,2] J. S. Halekas,[1,2] G. T. Delory,[1,2] W. M. Farrell,[2,3] V. Angelopoulos,[4] J. P. McFadden,[1] J. W. Bonnell,[1] and R. E. Ergun[5]

Received 14 November 2011; revised 1 December 2011; accepted 2 December 2011; published 4 January 2012.

[1] As an airless body in space with no global magnetic field, the Moon is exposed to both solar ultraviolet radiation and ambient plasmas. Photoemission from solar UV radiation and collection of ambient plasma are typically opposing charging currents and simple charging current balance predicts that the lunar dayside surface should charge positively; however, the two ARTEMIS probes have observed energy-dependent loss cones and high-energy, surface-originating electron beams above the dayside lunar surface for extended periods in the magnetosphere, which are indicative of negative surface potentials. In this paper, we compare observations by the ARTEMIS P1 spacecraft with a one-dimensional particle-in-cell simulation and show that the energy-dependent loss cones and electron beams are due to the presence of stable, non-monotonic, negative potentials above the lunar surface. The simulations also show that while the magnitude of the non-monotonic potential is mainly driven by the incoming electron temperature, the incoming ion temperature can alter this magnitude, especially for periods in the plasma sheet when the ion temperature is more than twenty times the electron temperature. Finally, we note several other plasma phenomena associated with these non-monotonic potentials, such as broadband electrostatic noise and electron cyclotron harmonic emissions, and offer possible generation mechanisms for these phenomena. **Citation:** Poppe, A. R., J. S. Halekas, G. T. Delory, W. M. Farrell, V. Angelopoulos, J. P. McFadden, J. W. Bonnell, and R. E. Ergun (2012), A comparison of ARTEMIS observations and particle-in-cell modeling of the lunar photoelectron sheath in the terrestrial magnetotail, *Geophys. Res. Lett.*, *39*, L01102, doi:10.1029/2011GL050321.

1. Introduction

[2] The surface of the Moon is exposed to a variety of ambient plasma, and in combination with solar ultraviolet-induced photoemission and the presence of surface remanent magnetic fields, determines the plasma environment immediately above the surface. Early theoretical work on the charging of exposed surfaces in space, including the Moon, Mercury and asteroids, quickly recognized that for some combinations of photoelectron and ambient plasma parameters, multiple solutions existed for the electrostatic potential structure above the surface [*Guernsey and Fu*, 1970; *Fu*, 1971; *Grard*, 1997; *Nitter et al.*, 1998]. These solutions were classified as being either monotonic, where the potential either steadily increases or decreases from infinity to the surface, or non-monotonic, where the potential is increasing in one region and decreasing in another. Simulations of photoelectric charging of spacecraft have indicated the likely presence of non-monotonic potentials in situations with large photoemission and a relatively tenuous ambient plasma [*Ergun et al.*, 2010]. These works also suggested, somewhat un-intuitively, that the non-monotonic potential may in fact be energetically preferred over the monotonic solution. In-situ measurements by the Lunar Prospector (LP) Electron Reflectometer (ER), which orbited the Moon and could sense the lunar surface potential via electron reflectometry, suggested that non-monotonic potentials were indeed present [*Halekas et al.*, 2008b, 2012]. By comparing with a one-dimensional particle-in-cell simulation, these measurements were confirmed as resulting from non-monotonic potentials [*Poppe and Horányi*, 2010; *Poppe et al.*, 2011].

[3] In this paper, we present a comparison of ARTEMIS P1 measurements of the lunar dayside plasma environment with one-dimensional particle-in-cell simulations of the lunar photoelectron sheath for an extended period in the terrestrial magnetotail. By making use of ARTEMIS' extensive suite of particles and fields instruments [*Angelopoulos*, 2012], including ion measurements (which were absent on LP), we are able to improve our particle-in-cell model and show excellent agreement with the ARTEMIS observations. This agreement significantly improves our understanding of the nature and variability of non-monotonic potentials and points to their likely ubiquity at airless bodies throughout the solar system. Additionally, we show that the presence of photoelectron beams associated with non-monotonic potentials generates large amounts of broadband electrostatic noise, most likely due to streaming instabilities.

2. ARTEMIS Observations

[4] The ARTEMIS mission consists of two identical probes in elliptical orbits around the Moon, with P1 orbiting prograde and P2 orbiting retrograde [*Angelopoulos*, 2012]. In this study, we focus on measurements by P1 on July 16,

[1]Space Sciences Laboratory, University of California, Berkeley, California, USA.
[2]NASA Lunar Science Institute, NASA Ames Research Center, Mountain View, California, USA.
[3]NASA Goddard Space Flight Center, Greenbelt, Maryland, USA.
[4]Department of Earth and Space Sciences and Institute of Geophysics and Planetary Physics, University of California, Los Angeles, California, USA.
[5]Laboratory for Atmospheric and Space Physics, University of Colorado at Boulder, Boulder, Colorado, USA.

0094-8276/12/2011GL050321

2011, of low-energy electrons and ions, and magnetic and electric field wave spectra, using the ElectroStatic Analyzer (ESA) [*McFadden et al.*, 2008], Electric Field Instrument (EFI) [*Bonnell et al.*, 2008] and Search Coil Magnetometer (SCM) [*Roux et al.*, 2008]. At this time, the Moon was located deep in the terrestrial magnetotail at GSE coordinates of approximately, [−59.5, −13.5, 3.80] R_E and the P1 orbit placed the spacecraft above the dayside lunar surface throughout the entire measurement period.

[5] Figure 1 shows an overview of P1 observations between 11:50 and 12:25 UTC, when the spacecraft was magnetically connected to the dayside lunar surface, assuming a straight-line extrapolation. While the incident energy flux is typical of the terrestrial magnetotail, the flux coming from the lunar surface is drastically different, showing both a relative deficit of high-energy electrons, which are lost to the lunar surface, and a cold beam of electrons accelerated up from the lunar surface. The beam energy varies throughout this time, including some periods in which the beam disappears, such as 11:59 to 12:01. In the magnetic and electric field FFT wave spectra, a host of electrostatic and electromagnetic waves are seen. From 11:50 to 11:58, and again from 12:01 to 12:14, both spectra show the presence of a narrow-band electromagnetic wave at frequencies varying between 30 and 200 Hz. These waves are most likely electromagnetic whistler waves, unrelated to the electrostatic potentials, and thus, we defer discussion of these to future work. The electric field FFT wave spectra show the presence of broadband electrostatic noise (BEN) throughout this time period, correlated with the presence of the up-going electron beam. Additionally, between approximately 11:57 and 12:00 there are a series of narrowband electrostatic emissions at approximate harmonics of the electron cyclotron frequency.

[6] Figures 2a and 2b show electron pitch angle-energy spectrograms in units of differential energy flux for two periods of distinctly different observations. Figure 2a shows the spectrogram at 11:59:39, with down-going plasma temperatures of T_e = 59 eV and T_i = 762 eV for electrons and ions, respectively, while Figure 2b shows the spectrogram at 12:04:04, with T_e = 247 eV and T_i = 1,310 eV. In both cases, the down-going plasma sheet electrons are isotropic, even at differing temperatures; however, the up-going spectra show distinct anisotropies as a result of combined electrostatic and magnetic reflection near the lunar surface [*Halekas et al.*, 2002, 2008b]. In both Figures 2a and 2b, an energy-dependent loss cone is seen for high-energy, field-aligned electrons that are absorbed by the lunar surface after penetrating both the lunar crustal remanent magnetic fields and the electrostatic potential. Additionally, both observations show up-going fluxes greater than the corresponding down-going flux at certain pitch angles and energies above the spacecraft potential (denoted as a vertical white line in Figures 2a and 2b). Below this potential, spacecraft-generated photoelectrons contaminate the detector [*Halekas et al.*, 2005]. In Figure 2a, the surface-originating flux manifests as an increase in up-going fluxes in the lowest non-contaminated bin centered at approximately 60 eV across 0–90° pitch angle, while in Figure 2b, the surface-originating flux is a cold beam at energies between 150–200 eV and pitch angles less than 30°. Spectra similar to Figure 2b have been previously shown to be indicative of negative, non-monotonic lunar surface potentials with respect to the ambient plasma [*Halekas et al.*, 2005, 2008b, 2011; *Poppe et al.*, 2011]. Figure 2a, in which the up-going photoelectrons do not develop into a focused beam in pitch angle, is still indicative of non-monotonic potentials, but at a much smaller magnitude than Figure 2b, assuming that the lunar photoelectrons are emitted as a roughly-Maxwellian distribution with a temperature of approximately 2.2 eV [*Feuerbacher et al.*, 1972].

3. Model / Data Comparisons

3.1. PIC Model Description and Results

[7] Previous comparisons between LP ER data and a one-dimensional particle-in-cell model of dayside negative surface potentials in the terrestrial plasma sheet have concluded that observations similar to Figures 1 and 2 are most likely due to the presence of stable, non-monotonic potential layers above the lunar surface [*Poppe et al.*, 2011; *Halekas et al.*, 2011]. In that study, only the electron parameters were explicitly measured, as LP lacked any ion instrumentation. With the use of ARTEMIS data, our model, as described by *Poppe and Horányi* [2010] and *Poppe et al.* [2011], can now be improved to include both the electron and ion temperatures, which are significantly different during this time period. Shown in Figure 3 is the PIC-modeled electrostatic potential as a function of height above the lunar surface for three values of the ion temperature, T_i = 500, 1000 and 2000 eV, with a constant electron temperature of T_e = 500 eV and density at infinity of $n_{ps} = 10^5$ m^{-3}. For all three cases, the potential is non-monotonic, yet with increasing ion temperature, the magnitude of the potential drop from infinity decreases as the ions provide more current to the surface. From the model results, we can derive an expression for the photoelectron beam energy, E_b, equivalent to the absolute value of the electrostatic potential drop from infinity to the minimum, as a function of the incoming ion and electron temperatures, T_e and T_i, given by,

$$E_b(T_e, T_i) = 0.712T_e - 0.053T_i + 5.92, \quad (1)$$

where all quantities are in units of eV. The incoming plasma sheet density, n_{ps}, does play a role in modulating the

Figure 1. ARTEMIS observations from a magnetically connected period on July 16, 2011, in the terrestrial magnetosphere. Shown are the differential energy flux for electrons coming up from (0−30° pitch angle) and going down to (90−180° pitch angle) the lunar surface, respectively, measured in eV/cm^2/s/str/eV, the downgoing ion and electron temperatures, the high-frequency FFT wave spectra for the magnetic and electric fields, respectively, the low frequency magnetic wavelet, the distance to the lunar surface along the magnetic field line in lunar radii, and the solar zenith angle (SZA), azimuthal (phi) and polar (theta) angles of the connected magnetic field line, assuming a straight-line extrapolation. Additionally, over-plotted in white on the differential electron energy fluxes (top two panels) is the spacecraft potential, over-plotted in red on the FFT spectra is the electron cyclotron frequency, and over-plotted in red on the wavelet is the proton cyclotron frequency. The two dashed lines denote individual observations shown in Figure 2.

electrostatic potential; however, the effect is negligible for these observations as the density varied within a factor of two, compared to the temperatures, which have variations of approximately an order of magnitude.

3.2. Comparison to ARTEMIS Data

[8] To explicitly compare the model predictions with the ARTEMIS observations, we use equation (1) with the ARTEMIS-measured T_e and T_i as a function of time to yield

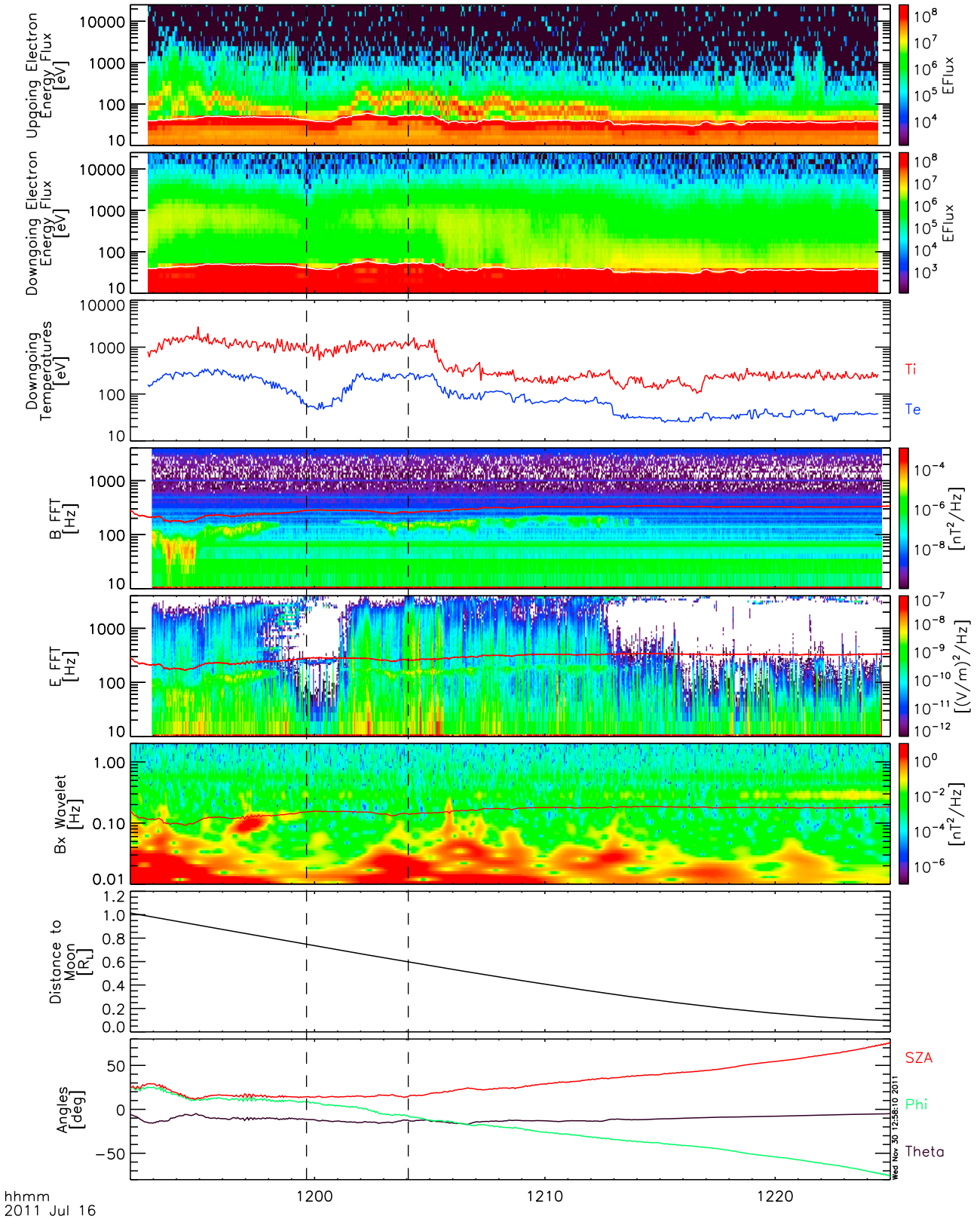

Figure 1

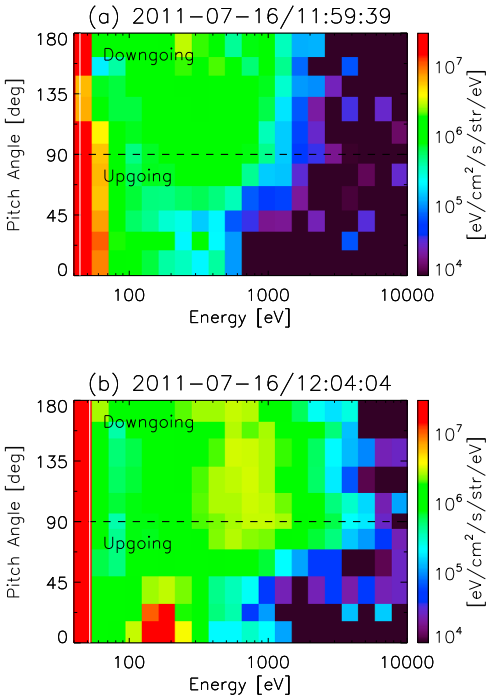

Figure 2. Electron pitch angle-energy spectrograms shown in units of differential electron energy flux for two time periods, (a) 11:59:39 and (b) 12:04:04. The spacecraft potential for each case is plotted as the vertical white line.

a PIC model-predicted beam energy as a function of time. Figure 4 (top) shows the ratio of up-going to down-going electron differential energy flux with the PIC model-predicted beam energy (summed with the spacecraft potential), for two conditions: (1) $T_i \equiv T_e$ (red line), and (2) T_i equivalent to the true ion temperature, as measured by ARTEMIS (black line). The PIC model-predicted beam energies for both conditions show excellent agreement with the observed beam, especially for times between 12:02 and 12:25, where the ion temperature is only two to five times the electron temperature. For times earlier than 11:59, the observed beam appears at energies slightly less than the predicted value. During this time, there are indications of electromagnetic wave activity near the proton cyclotron frequency, which is indicative of ion dynamics, perhaps due to ions of lunar origin; however, the Moon was in the magnetotail and no significant convection electric field exists to pick up any ions generated near the lunar surface (via photoionization or sputtering, for example) and accelerate them to measurable energies. Nonetheless, one plausible mechanism that could couple the presence of multiple ion species and the cold photoelectron beam is the generation of electromagnetic ion cyclotron waves, as described by *Temerin and Lysak* [1984]. Indeed, the observed deviations of the photoelectron beam energy from the model may be telling us about near-surface particle populations and dynamics.

[9] While the photoelectron beam is a prominent effect throughout most of this time period, it does disappear, in agreement with the PIC model, from approximately 11:59–12:02. Concurrent with this time period, the plasma sheet electron temperature (third panel of Figure 1) decreases smoothly from approximately 200 eV to a minimum around 50 eV before smoothly increasing back to its previous value. The plasma sheet ion temperature remains relatively constant during this time at approximately 1000 eV. By setting the left-hand side of equation (1) equal to zero, we can determine values of T_e and T_i for which the predicted beam energy is less than or equal to zero (implying that the beam vanishes). By first defining the temperature ratio, $R = T_i/T_e$, we solve equation (1) for a somewhat implicit, model-predicted condition for the beam to vanish, given by,

$$R > 13.4 + 111.7\frac{1}{T_e}. \quad (2)$$

[10] Figure 4 (middle) shows the temperature ratio as a function of time, with a critical ratio, defined by $R_C = 13.4 + 111.7T_e^{-1}$, over plotted in red. During most of this time, the temperature ratio is below the critical value and the beam is seen in the up-going energy fluxes. Commensurate with the decrease of the incoming electron temperature, the ratio increases above R_C and correspondingly, both the model and the data show the beam disappear, although, there does exist a small amount of un-focused, upward energy flux in the lowest energy bins above the spacecraft potential that serves to balance the plasma sheet current to the lunar surface. During this time, the plasma sheet electron current to the lunar surface decreases as the electron temperature decreases and thus, the net current to the lunar surface increases. The non-monotonic potential correspondingly decreases in magnitude to reduce the incoming ion current and maintain current balance at the surface, to the extent that the photoelectrons escaping from the lunar surface no longer experience significant acceleration and pitch-angle focusing as they travel up to the spacecraft (see Figure 2a).

[11] Finally, Figure 4 (bottom) shows the electric field wave power in the 732 Hz bin, which, based on Figure 1, can be used as a proxy for the presence of BEN. The BEN is present at times when the beam is at relatively high energies, yet ceases when the beam has either disappeared (11:59–12:01) or when the beam is at a very low energy level (12:13–12:25). One possible mechanism for the generation of both the BEN and the previously mentioned electron cyclotron harmonic emissions may be the coupling of the electron

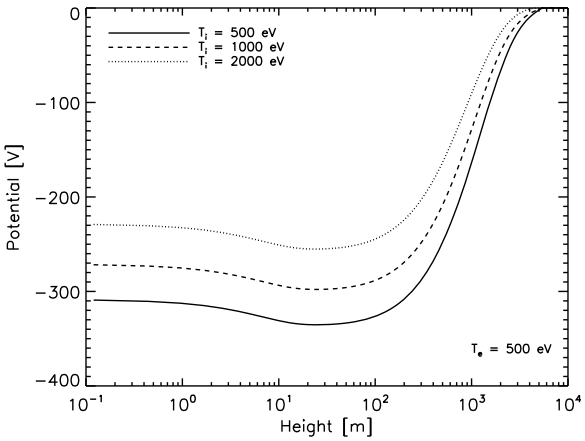

Figure 3. The potential as a function of height above the lunar surface from the PIC model for three different cases of plasma sheet ion temperature, T_i = 500, 1000, 2000 eV, for constant electron temperature, T_e = 500 eV, and density, $n_{ps} = 10^5$ m^{-3}.

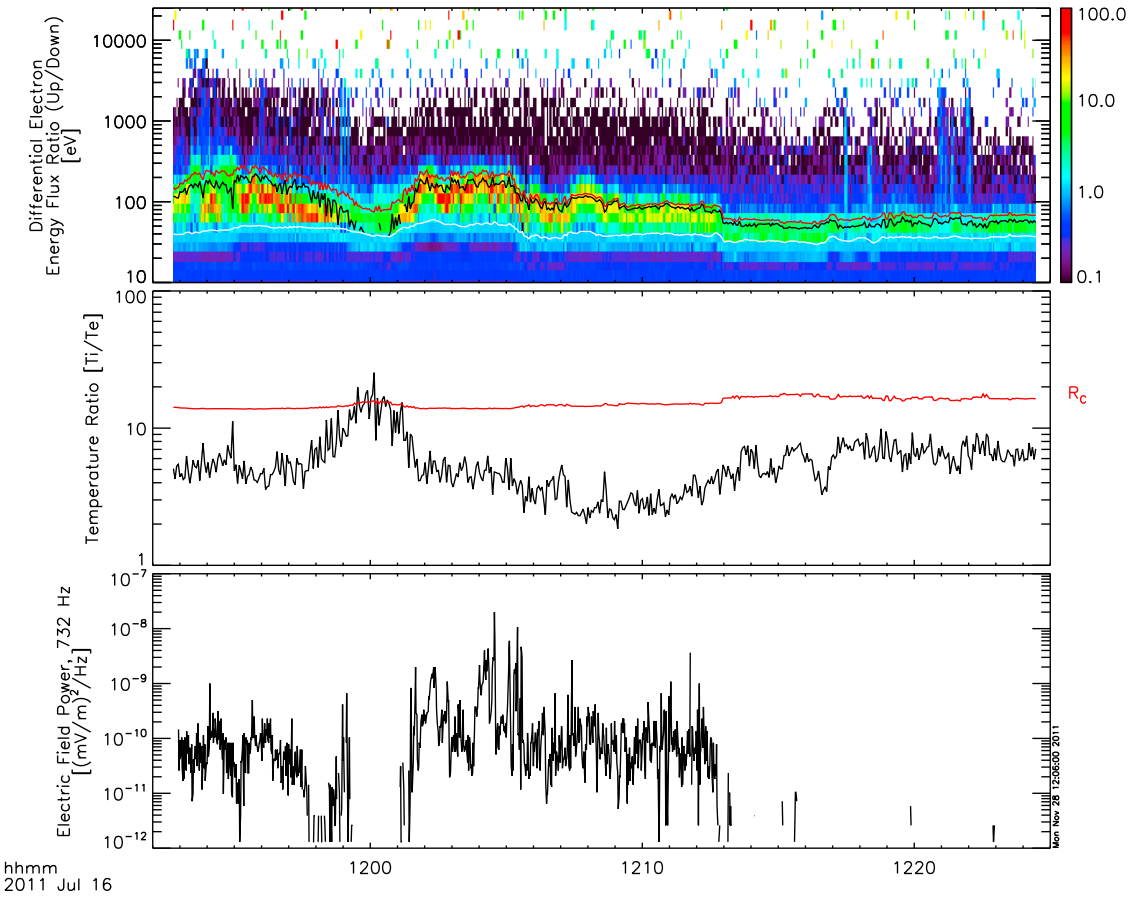

Figure 4. (top) The up-going to down-going differential electron energy flux ratio with the model-predicted beam energy with $T_i \equiv T_e$ and the true T_i taken from ARTEMIS measurements (red and black lines, respectively), and the spacecraft potential (white line) over-plotted, (middle) the temperature ratio (T_i/T_e) with the critical ratio, R_C, as defined in the text (red line), and (bottom) the electric field wave power in the 732 Hz bandpass for the same time period as Figure 1.

acoustic instability from the streaming photoelectrons and the instability of the loss cone anisotropy, similar to that outlined by *Roeder et al.* [1991], especially given the high degree of correlation between the BEN and the presence of the photoelectron beam. We suggest that the presence of both BEN and electron cyclotron harmonic emissions near airless bodies can be used as a diagnostic in searching for surface-generated electron beams and possible non-monotonic potentials at other airless bodies [*Gurnett et al.*, 1981; *Kurth et al.*, 1987, 2001; *Santolík et al.*, 2011].

4. Summary

[12] We have presented measurements by ARTEMIS P1 of energy-dependent loss cones and cold, up-going field-aligned beams of photoelectrons, both of which indicate that the dayside lunar surface is at a negative potential with respect to the spacecraft. Using a one-dimensional particle-in-cell code, we have shown that these measurements are due to stable, non-monotonic potentials that arise due to the interaction of the lunar photoelectron and terrestrial plasma sheaths. The extended time period and plasma temperature range over which the PIC model agrees with the ARTEMIS measurements significantly improves our understanding of non-monotonic potentials above airless bodies, which has previously only been compared for a single Lunar Prospector measurement [*Poppe et al.*, 2011]. Indeed, the wide temperature range over which the PIC model has now been validated against in-situ observations, from 10 eV in the solar wind [*Poppe and Horányi*, 2010; *Halekas et al.*, 2011] to over 1 keV in the terrestrial plasma sheet [*Poppe et al.*, 2011], implies that non-monotonic potentials may exist at nearly all airless, non-magnetized bodies throughout the solar system. The presence of a multitude of electrostatic and electromagnetic waves associated with the non-monotonic potentials, loss cones, and photoelectron beam further enriches this environment, and provides additional means of searching for non-monotonic potentials throughout the solar system. We suggest that these phenomena are not unique to the Moon and should occur at many airless bodies, including Mercury, asteroids, and the moons of the giant planets [*Grard*, 1997; *Roussos et al.*, 2010; *Santolík et al.*, 2011]. The non-monotonic potentials also have implications for other lunar-related phenomena, including the electrostatic levitation of micron-sized dust grains [*Poppe and Horányi*, 2010; *Grün et al.*, 2011] and the interaction of plasma with lunar crustal remanent magnetic fields [*Harnett and Winglee*, 2003; *Halekas et al.*, 2008a]. Finally, we also suggest that the continuous presence of such non-monotonic potentials, and the complex electric fields that these potentials give rise to, may have significant effects on the trajectories and

densities of sputtered and photo-ionized pick-up ions above the dayside lunar surface.

[13] **Acknowledgments.** The authors gratefully acknowledge support from NASA's Lunar Science Institute. The ARTEMIS mission was funded and is operated under NASA grant NAS5-02099. The authors thank E. M. Harnett and another anonymous reviewer for helpful and constructive comments.

[14] The Editor thanks Erika Harnett and an anonymous reviewer for their assistance in evaluating this paper.

References

Angelopoulos, V. (2012), The ARTEMIS mission, *Space Sci. Rev.*, in press.

Bonnell, J. W., et al. (2008), The electric field instrument (EFI) for THEMIS, *Space Sci. Rev.*, *141*, 303–341.

Ergun, R. E., et al. (2010), Spacecraft charging and ion wake formation in the near-Sun environment, *Phys. Plasma*, *17*, 072903, doi:10.1063/1.3457484.

Feuerbacher, B., et al. (1972), Photoemission from lunar surface fines and the lunar photoelectron sheath, *Proc. Lunar Sci. Conf.*, *3*, 2655–2663.

Fu, J. H. M. (1971), Surface potential of a photoemitting plate, *J. Geophys. Res.*, *76*(10), 2506–2509.

Grard, R. (1997), Photoemission on the surface of Mercury and related electrical phenomena, *Planet. Space Sci.*, *45*, 67–72.

Grün, E., et al. (2011), The lunar dust environment, *Planet. Space Sci.*, *59*, 1672–1680.

Guernsey, R. L., and J. H. M. Fu (1970), Potential distribution surrounding a photo-emitting, plate in a dilute plasma, *J. Geophys. Res.*, *75*(16), 3193–3199.

Gurnett, D. A., et al. (1981), Narrowband electromagnetic emissions from Saturn's magnetosphere, *Nature*, *292*, 733–737.

Halekas, J. S., D. L. Mitchell, R. P. Lin, L. L. Hood, M. H. Acuña, and A. B. Binder (2002), Evidence for negative charging of the lunar surface in shadow, *Geophys. Res. Lett.*, *29*(10), 1435, doi:10.1029/2001GL014428.

Halekas, J. S., R. P. Lin, and D. L. Mitchell (2005), Large negative lunar surface potentials in sunlight and shadow, *Geophys. Res. Lett.*, *32*, L09102, doi:10.1029/2005GL022627.

Halekas, J. S., et al. (2008a), Solar wind interaction with lunar crustal magnetic anomalies, *Adv. Space Res.*, *41*, 1319–1324.

Halekas, J. S., G. T. Delory, R. P. Lin, T. J. Stubbs, and W. M. Farrell (2008b), Lunar Prospector observations of the electrostatic potential of the lunar surface and its response to incident currents, *J. Geophys. Res.*, *113*, A09102,doi:10.1029/2008JA013194.

Halekas, J. S., et al. (2012), Solar wind electron interaction with the dayside lunar surface and crustal magnetic fields: Evidence for precursor effects, *Earth Planets Space*, in press.

Harnett, E. M., and R. M. Winglee (2003), 2.5-D fluid simulations of the solar wind interacting with multiple dipoles on the surface of the Moon, *J. Geophys. Res.*, *108*(A2), 1088, doi:10.1029/2002JA009617.

Kurth, W. S., D. D. Barbosa, D. A. Gurnett, and F. L. Scarf (1987), Electrostatic waves in the magnetosphere of Uranus, *J. Geophys. Res.*, *92*(A13), 15,225–15,233.

Kurth, W. S., et al. (2001), The plasma wave environment of Europa, *Planet. Space Sci.*, *49*, 345–363.

McFadden, J. P., et al. (2008), The THEMIS ESA plasma instrument and in-flight calibration, *Space Sci. Rev.*, *141*, 277–302.

Nitter, T., O. Havnes, and F. Melandsø (1998), Levitation and dynamics of charged dust in the photoelectron sheath above surfaces in space, *J. Geophys. Res.*, *103*(A4), 6605–6620.

Poppe, A., and M. Horányi (2010), Simulations of the photoelectron sheath and dust levitation on the lunar surface, *J. Geophys. Res.*, *115*, A08106, doi:10.1029/2010JA015286.

Poppe, A., J. S. Halekas, and M. Horányi (2011), Negative potentials above the day-side lunar surface in the terrestrial plasma sheet: Evidence of non-monotonic potentials, *Geophys. Res. Lett.*, *38*, L02103, doi:10.1029/2010GL046119.

Roeder, J. L., V. Angelopoulos, W. Baumjohann, and R. R. Anderson (1991), Observations of correlated broadband electrostatic noise and electron cyclotron emissions in the plasma sheet, *Geophys. Res. Lett.*, *18*(1), 53–56.

Roussos, E., N. Krupp, H. Krüger, and G. H. Jones (2010), Surface charging of Saturn's plasma-absorbing moons, *J. Geophys. Res.*, *115*, A08225, doi:10.1029/2010JA015525.

Roux, A., et al. (2008), The search coil magnetometer for THEMIS, *Space Sci. Rev.*, *141*, 265–275.

Santolík, O., D. A. Gurnett, G. H. Jones, P. Schippers, F. J. Crary, J. S. Leisner, G. B. Hospodarsky, W. S. Kurth, C. T. Russell, and M. K. Dougherty (2011), Intense plasma wave emissions associated with Saturn's moon Rhea, *Geophys. Res. Lett.*, *38*, L19204, doi:10.1029/2011GL049219.

Temerin, M., and R. L. Lysak (1984), Electromagnetic ion cyclotron mode (ELF) waves generated by auroral electron precipitation, *J. Geophys. Res.*, *89*(A5), 2849–2859.

V. Angelopoulos, Department of Earth and Space Sciences, University of California, Box 951567, Los Angeles, CA 90095, USA.

J. W. Bonnell, G. T. Delory, J. S. Halekas, J. P. McFadden, and A. R. Poppe, Space Sciences Laboratory, University of California, 7 Gauss Way, Berkeley, CA 94720, USA. (poppe@ssl.berkeley.edu)

R. E. Ergun, Laboratory for Atmospheric and Space Physics, University of Colorado at Boulder, Campus Box 530, 1234 Innovation Dr., Boulder, CO 80303, USA.

W. M. Farrell, NASA Goddard Space Flight Center, Code 695, Greenbelt, MD 20771, USA.